Geoneutrinos: Using Particle Physic to Understand and Image the Earth

Kyaw Linn Zaw[1#], Ondrej Sramek[2], William F. Mc Donough[3] and Fabio Mantovani[4]

Abstract

A geoneutrino is a neutrino or antineutrino emitted in decay of radionuclide naturally occurring in the Earth. Matter is virtually transparent to neutrinos and consequently they travel, unimpeded, at near light speed through the Earth from their point of emission. Collectively, geoneutrinos carry integrated information about the abundances of their radioactive sources inside the Earth. Most geoneutrinos are electron antineutrinos originating in β^- decay branches of ^{40}K, ^{232}Th and ^{238}U. Together these decay chains account for more than 99% of the present-day radiogenic heat generated inside the Earth. The Earth has cooled since its formation, the current total heat flux from the Earth to space is 44.2±1.0 TW, but the relative contributions from residual primordial heat and radiogenic decay remain uncertain. Precise measurements of the geoneutrino flux from the Kamioka Liquid-Scintillator Antineutrino Detector, Japan, with existing measurements from the Borexino detector, Italy find that decay of ^{238}U and ^{232}Th together contribute 20.0±8.6 TW to Earth's heat flux. The observations indicate that heat from radioactive decay contributes about half of Earth's total heat flux. These radioactivity in the Earth mantle provides internal heating to power mantle convection, which is the driver of plate tectonics. We therefore conclude that Earth's primordial heat supply has not yet been exhausted.

Keywords: geoneutrinos, heat flux, radiogenic heat, primordial heat

Introduction

Neutrinos, the lightest of the known subatomic particles, lack measurable electromagnetic properties and interact only via the weak nuclear force when ignoring gravity. Matter is virtually transparent to neutrinos and consequently they travel, unimpeded, at near light speed through the Earth from their point of emission. Collectively, geoneutrinos carry integrated information about the abundances of their radioactive sources inside the Earth. A major objective of the emerging field of neutrino geophysics involves extracting geologically useful information (e.g., abundances of individual geoneutrino-producing elements and their spatial distribution in Earth's interior) from geoneutrino measurements.

Most geoneutrinos are electron antineutrinos originating in β^-decay branches of ^{40}K, ^{232}Th and ^{238}U. Together these decay chains account for more than 99% of the present-day radiogenic heat generated inside the Earth. Only geoneutrinos from ^{232}Th and ^{238}U decay chains are detectable by the inverse beta-decay mechanism on the free proton because these have energies above the corresponding threshold (1.8 MeV). In neutrino experiments, large underground liquid scintillator detectors record the flashes of light generated from this interaction. As of 2016 geoneutrino measurements at two sites, as reported by the KamLAND and Borexino collaborations, have begun to place constraints on the amount of radiogenic heating in the Earth's interior. A third detector (SNO+) is expected to start collecting data in 2017. JUNO experiment is under construction in Southern China. Another geoneutrino detecting experiment is planned at the China Jinping Underground Laboratory.

[1]Lecturer, Department of Geology, West Yangon University
[2]Geophysicist, Department of Geophysics, Charles University, Czech Republic
[3]Professor, Department of Geology, University of Maryland, USA
[4]Professor, Department of Physics and Earth Sciences, University of Ferrara, Italy
#Corresponding Author: klinzaw@gmail.com

Geoneutrinos detection

Already in 1946 Bruno Pontecorvo (Pontecorvo *et al*., 1946) suggested to use nuclear reactors in order to perform neutrino experiments. Indeed, in 1953-1959 Reines and Cowan (Cowan *et al*., 1956) showed that anti-neutrinos are real particles using nuclear reactors as a source. Since then, nuclear reactors have been extensively used to study neutrino properties. The KamLAND experiment represents the culmination of a fifty year effort, all using the same method which was applied by Reines and Cowan. The inverse β-decay reaction, $\bar{\nu}_e + p \rightarrow e + n$ (where νe and p in the left side are theanti-neutrino and proton, respectively, e^+ and n in the right side denote the neutron and positron, respectively), is used to detect $\bar{\nu}_e$'s with energies above 1.8 MeV in liquid scintillator. The prompt signal from the positron and the 2.2 MeV γ-ray from neutron capture on a proton in delayed coincidence provide a powerful tool for reducing background and to reveal the rare interaction of antineutrinos (Fig. 1). The primary goal of KamLAND was a search for the oscillation of $\bar{\nu}_e$'s emitted from distant power reactors. The long baseline, typically 180 km, enabled KamLAND to address the oscillation solution of the 'solar neutrino problem' using reactor anti-neutrinos. KamLAND has been able to measure the oscillation parameters of electron anti-neutrinos, by comparing the observed event spectrum with that predicted in the absence of oscillation. In addition, KamLAND was capable to extract the signal of geo-neutrinos from ^{238}U and ^{232}Th. Due to the different energy spectra, events from Uranium and Thorium progenies can be separated. The best fit attributes 4 events to ^{238}U and 5 to ^{232}Th. According to (Eguchi *et al*., 2003) and (Raghavan *et al*., 1998), this corresponds to about 40 TW radiogenic heat generation, values from 0 to 110 TW being allowed at 95% C.L.

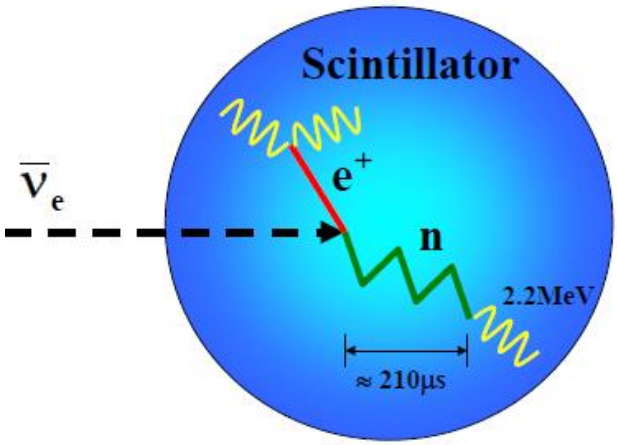

Figure (1) The signature of inverse β-decay, $\nu_e + p \rightarrow e + n$. Energy released in the slowing down of the positron and the two γ's from positron annihilation is the prompt signal, followed by the 2.2 MeV γ-ray from neutron capture on a proton.

The reference model of geoneutrino production

The main sources of heat and antineutrinos in the Earth's interior are Uranium, Thorium and Potassium. Through its decay chain, each nuclide releases energy together with anti- neutrinos (Table 1). From the distribution of these elements in the Earth one can thus estimate both radiogenic heat flow and the anti-neutrino flow.

Table (1) Main radiogenic sources. We report the Q-values, the half-lives ($\tau 1/2$), the maximal energies ($Emax$), heat and anti-neutrino production rates (ε_H mass for natural isotopic abundances and ε_ν) per unit

Decay		Q	$\tau_{1/2}$	E_{max}	ε_H	ε_ν
		(MeV)	(10^9 yr)	(MeV)	(W/kg)	($kg^{-1}s^{-1}$)
$^{238}U \rightarrow {}^{206}P$	$b + 8\ {}^4He + 6e + 6\nu$	51.7	4.47	3.26	$0.95 \cdot 10^{-4}$	$7.41 \cdot 10^{7}$
$^{232}Th \rightarrow {}^{208}Pb$	$Pb + 6\ {}^4He + 4e + 4\nu$	42.8	14.0	2.25	$0.27 \cdot 10^{-4}$	$1.63 \cdot 10^{7}$
$^{40}K \rightarrow {}^{40}C$	$a + e + \nu$	1.32	1.28	1.31	$0.36 \cdot 10^{-8}$	$2.69 \cdot 10^{4}$

Recently, a reference model of geo-neutrino fluxes has been presented in (Mantovani *et al*., 2004). The main ingredients of this model and its predictions for geo-neutrino fluxes and event yields are reviewed in the following. World-averaged abundances of radiogenic elements have been estimated separately for oceans, the continental crust (subdivided into upper, middle and lower sub-layers), sediments, and oceanic crust. Although this treatment looks rather detailed on the globe scale, the typical linear dimension of each tile is of order 200 km, so that any information on a smaller scale is essentially lost. The Preliminary Reference Earth Model (Dziewonski *et al*., 1981) was used for the mantle density profile, dividing Earth's interior into several spherically symmetrical shells corresponding to seismic discontinuities. Concerning its composition, a two-layer stratified model was used: for present day upper mantle, considered as the source of MORB, mass abundances of 6.5 and 17.3 ppb for Uranium and Thorium respectively and 78 ppm for Potassium were assumed down to a depth h_0 = 670 km. These abundances were obtained by averaging the results of Refs. (Jochum *et al*., 1983) and (Zartman *et al*., 1988). Abundances in the lower mantle were inferred by requiring that the BSE constraint is globally satisfied, thus obtaining 13.2 and 52 ppb for U and Th respectively, 160 ppm for K.

We concentrate here on a few locations of specific interest:

(i) For the Kamioka mine, where the KamLAND detector is in operation, the predicted uranium flux is $\Phi_U = 3.7 \cdot 10^6$ $cm^{-2}s^{-1}$, the flux from Thorium is comparable and that from Potassium is fourfold. Within the reference model, about 3/4 of the flux is generated from material in the crust and the rest mainly from the lower mantle.

(ii) At Gran Sasso laboratory, where Borexino (Alimonti et al., 2002) is in preparation, the prediction is $\Phi_U = 4.2 \cdot 10^6$ $cm^{-2}s^{-1}$, this larger flux arising from a bigger contribution of the surrounding continental crust. Thorium and Potassium fluxes are found to be correspondingly rescaled.

(iii) At the top of Himalaya, a place chosen so that the crust contribution is maximal, one has $\Phi_U = 6.7 \cdot 10^6$ $cm^{-2}s^{-1}$. The crust contribution exceeds 90%.

(iv) At Hawaii, a site which minimizes the crust contribution, the prediction is $\Phi_U = 1.3 \cdot 10^6$ $cm^{-2}s^{-1}$, originated mainly from the mantle.

From the produced fluxes, together with the knowledge of neutrino propagation (*i.e.* the oscillation parameters), the interaction cross section and the size of the detector, one can compute the expected event yields. These are shown over the globe in figure (2) (see http://www.neogeo.unisi.it/fabio/index.asp for more information). In summary, this reference model has to be intended as a starting point, providing first estimates of expected fluxes and events. In view of the present debate about mantle circulation and composition, a

more general treatment is needed, which encompasses both geochemically and geophysically preferred models.

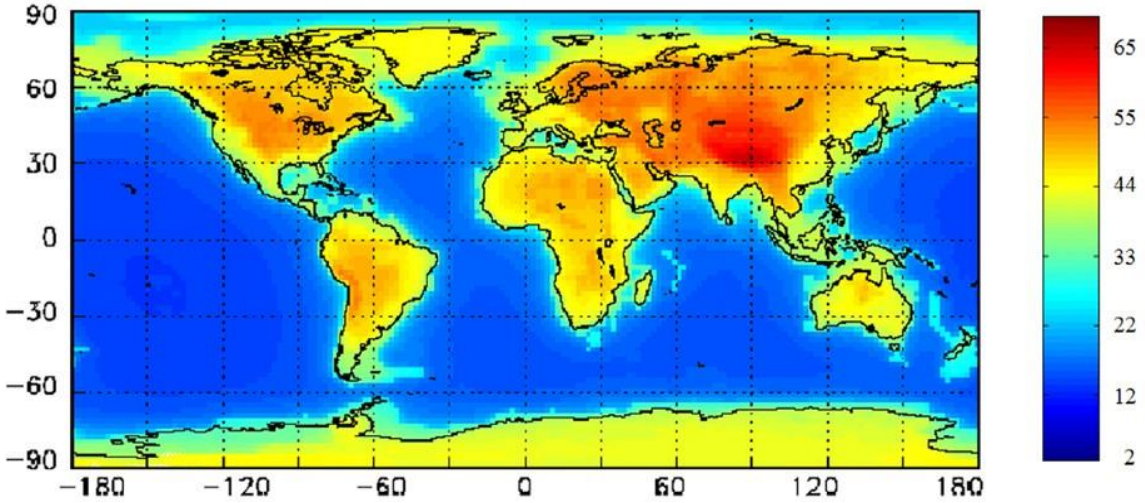

Figure (2). Predicted geo-neutrino events from Uranium and Thorium decay chains, normalized to 10^{32} protons yr and 100% efficiency.

The effects of local structures

The main result of the previous section is that - neglecting regional fluctuations global mass balance provides a precise determination of the geo-neutrino fluxes. We shall compare this precision with uncertainties resulting from fluctuations of the regional geochemical composition.

Indeed the Uranium concentration in the region where the detector is located may be different from the world average and local fluctuations of this highly mobile element are to be envisaged. These variations, although negligible for mass balance, can affect the flux significantly. In other words, geometrical arguments fix the contribution of distant sources and a more detailed geological and geochemical investigation of the region around the detector is needed.

The contribution from the crust near KamLAND

It has been estimated that about one half of the geo-neutrino signal is generated within a distance of 500 km from Kamioka, essentially in the Japanese continental shelf. In REF the world averaged upper crust Uranium concentration, $a_{uc} = 2.5\,ppm$, was adopted for Japan. In a recent study of the chemical composition of Japan upper crust (Togashi *et al.*, 2000) more than hundred samples, corresponding to 37 geological groups, have been analyzed. The composition is weighted with the frequency in the geological map and the resulting average abundance is $a_{Jap} = 2.32\,ppm$, which implies a 7.2% reduction of the flux from Japanese upper crust with respect to that estimated in REF. Larger variations occur when rocks are divided according to age or type (Table 2), and even larger differences are found within each group. All this calls for a detailed geochemical and geophysical study, with the goal of reducing the effect of regional fluctuations to the level of the uncertainty from global geochemical constraints.

Table (2). Uranium abundances in the upper continental crust of Japan. Groups correspond to rock's age or type and quoted abundances for each group are area weighted values, from Ref. (Albarede, 2003).

Group	**Area %**	a_{uc} **(ppm)**
Pre-Neogene	41.7	2.20
Pre-Cretaceous	10.5	2.11
Neog-Quat. Igneous rocks	24.1	2.12
Paleog-Cret. Igneous rocks	14.1	3.10
Sedimentary	39.9	2.49
Metamorphic	21.3	1.72
Igneous	38.4	2.48
Global area weighted average	**99.6**	**2.32**

The subducting slab below the Japan Arc

As well known, below the Japan islands arc there is a subducting slab originating from the Philippine and Pacific plates. Let us compare the amount of Uranium carried by this plate with that contained in the continental crust of the Japan arc.

Roughly, the Japan crust can be described as a rectangle with area $A=L_1 \cdot L_2 \approx$ 1800x250 km^2 = 4.5·10^5 km^2 (Fig. 3). Conrad depth is on the average at h_1=18km and Moho discontinuity at h_2=36 km (Zhao *et al*., 1992). We assume uniform density ρ=2.7 ton/m^3. Concerning Uranium abundance we take for the upper crust a_{uc}=2.3 ppm from (Togashi *et al*., 2000). For the lower crust we take a_{lc}= 0.6 ppm, an average between largely different estimates. The resulting uranium masses, $m_i = A\, h\, \rho\, a_i$, are reported in table (3).

Table (3). Estimate for the uranium mass in the continental crust of Japan Island arc.

	Crustal Mass (10^{19} Kg)	**Uranium abundance (10^{-6})**	**Uranium Mass (10^{13} kg)**
Upper crust	2.2	2.3	5.0
Lower crust	2.2	0.6	1.3
Total	**4.4**		**6.3**

The Philippine plate is moving towards the Eurasia plate at about 40 mm/yr and is subducting beneath the southern part of Japan. The Pacific Plate is moving in roughly the same direction at about 80 mm/yr and is subducting beneath the northern half of Japan. The slab is penetrating below Japan with an angle α≈6° with respect to the horizontal. This process has been occurring on a time scale T≈108 y. Along this time the slab front has advanced by D=vT≈6000 km for v=60 mm/yr, the average of the two plates (Fig. 4). We assume that the slab brings with it oceanic crust, with density ρ*oc*=3 Ton/m3 for a depth *h3*≈10 km, the Uranium abundance being typical of an oceanic crust, *aoc*=0.1 ppm.

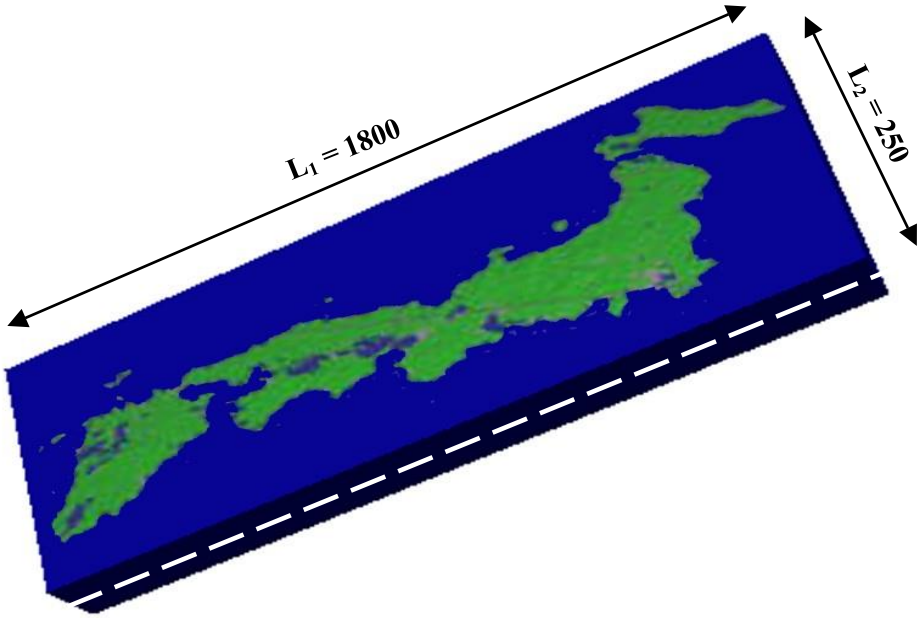

Figure (3). A sketch of the Japan Island Arc.

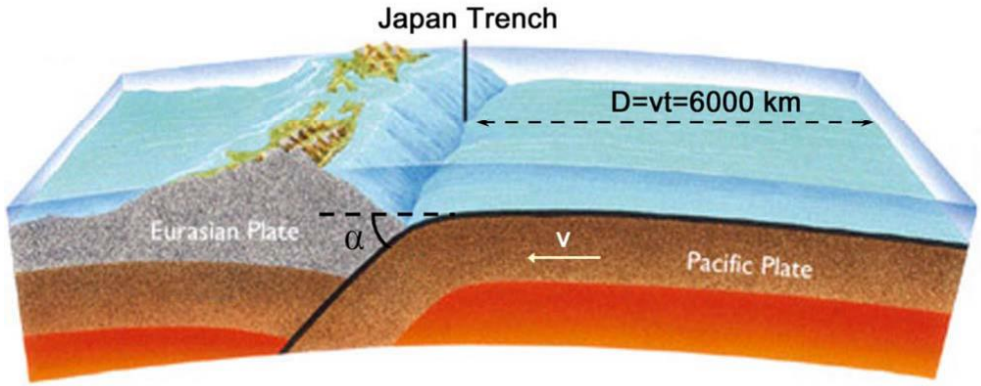

Figure (4). A sketch of the Japan arc continental crust and of the subducting slab beneath. The subduction angle is $\alpha \approx 6^{\circ}$

If we assume that the slab keeps its trace elements while subducting, we have just to estimate the amount of Uranium which is contained in the subducting crust below Japan. Its area A' below is slightly larger than that of Japan arc, A' = A cosα ≈ A. For the assumed values of density and depth the mass of the slab is M_{slab} = 1.35 10^{19} kg. The Uranium mass in the subducting crust is thus m_{slab}= 1.3 10^{12} kg, a negligible amount as it is about 1/40 of that in the continental crust of Japan.

On the other hand, it is possible that the slab loses Uranium while subducting. As an extreme case, we assume that all Uranium from the subducting crust is dissolved in fluids during dehydration reactions and accumulates in the lower part of the continental crust of Japan, enriching it. Since Japan has been exposed to a slab of length $D \approx$ 6000 km, the maximal accumulated Uranium mass is m_{acc}=3.2 10^{13}kg. This corresponds to an increase of the Uranium abundance in the Japanese lower continental crust, which becomes a_{lc}=2 ppm instead of the previously assumed 0.6 ppm. The prediction of the produced flux at

Kamioka changes from 3.7 to 4.0 10^6 cm^{-2} s^{-1}. We remark that this 8% effect has been derived assuming the extreme hypothesis of a complete release.

Discussion

Two observations of the surface geoneutrino signal by detectors separated by about 120_ of longitude in the Northern Hemisphere now exist. Systematic uncertainty of the background limits the precision of the KamLAND observation, while low statistics limits the precision of the Borexino observation. The resulting precisions of about 40% do not allow measurement of the thorium-to-uranium mass ratio. Assuming the observations exhibit a specific thoriumto- uranium mass ratio (Th/U = 3.9), allows assessments of terrestrial radiogenic heating.

In general, higher geoneutrino signal rates indicate higher levels of radiogenic heating. However, the distribution of U and Th within the mantle influences the geoneutrino signal. The maximum signal results from a homogeneous distribution, assuming abundances of U and Th do not decrease with depth in the mantle. The minimum signal places as much U and Th in an enriched layer at the base of the mantle (D″) as allowed by a depleted mantle with depleted MORB source mantle composition. Figure (5a) compares the maximum and minimum mantle geoneutrino signals with the combined observations of KamLAND and Borexino as a function of U and Th enrichment. This comparison demonstrates the potential to exclude enrichment parameters using measurements of the mantle geoneutrino signal rate. Additional leverage results from measurements of the mantle geoneutrino signal Th/U ratio. This follows from the superchondritic Th/U ratio (Th/U ≈ 4.3) in continental crust, forcing a subchondritic Th/U ratio in the depleted mantle. Figure (5b) shows the dependence of the Th/U signal ratio on U and Th enrichment bound by the mantle distributions for maximum and minimum signal rate.

The preceding discussion describes how the radiogenic heating indicated by a geoneutrino signal depends on the assumed distribution of U and Th within the mantle. Figure (6) compares the minimum and maximum radiogenic heating assessments of KamLAND and Borexino with the predictions of the geological models and with the surface heat flow. The KamLAND result assuming a homogenous distribution of U and Th in the mantle (minimum radiogenic heating), suggesting the presence of primordial heat loss, mildly excludes the synthetic fully radiogenic model and the high end-member of the geophysical model. These exclusions do not hold for the KamLAND result assuming an enriched layer at the base of the mantle (maximum radiogenic heating).

The Borexino result (both maximum and minimum), implying radiogenic heating in the silicate earth >29 TW, excludes the presence of primordial heat loss, the cosmochemical model, and the low end-member of the geophysical model. However, the Borexino result, which is based on relatively small statistics, carries large uncertainties. Assuming both the KamLAND and Borexino observatories sample identical mantle signals allows combining the two results in a weighted average. The combined result, assuming a homogeneous mantle, mildly excludes the synthetic fully radiogenic model and the low end-member of the cosmochemical model. Assuming an enriched layer retains the mild exclusion of the low end-member of the cosmochemical model and loses the exclusion of the synthetic fully radiogenic model.

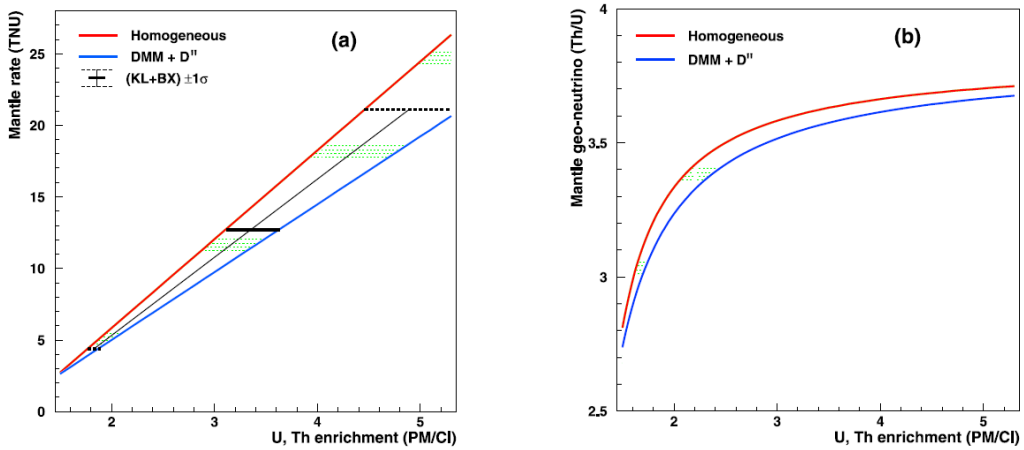

Figure (5). **(a)** The variation of mantle geoneutrino rate as a function of primitive mantle enrichment of refractory heatproducing elements (U, Th) for a homogeneous distribution (maximum rate) and for DMM with U and Th composition given by Salters and Stracke (2004) overlying an enriched layer (D″) at the base of the mantle (minimum rate). For comparison, the combined geoneutrino result (KL + BX) with uncertainty is plotted over the allowed space. **(b)** The variation of mantle geoneutrino Th/U ratio as a function of primitive mantle enrichment of refractory heat producing elements (U, Th) for a homogeneous distribution (maximum rate) and for DMM with U and Th composition given by Salters and Stracke (2004) overlying an enriched layer at the base of the mantle (minimum rate). The green shaded area between the curves specifies the allowed parameter space.

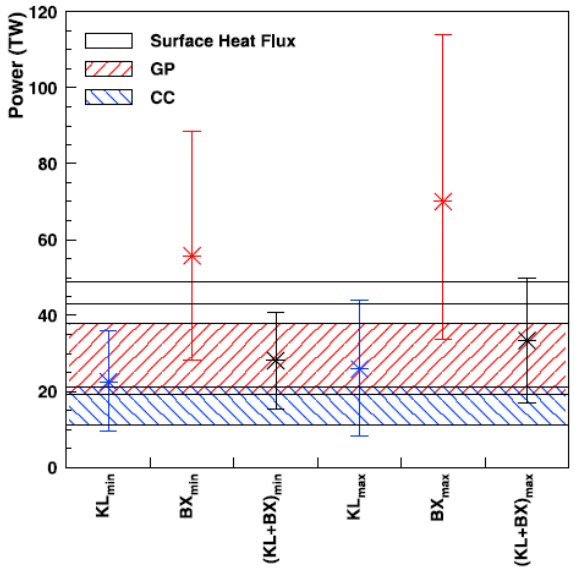

Figure (6). Comparison of the radiogenic heating implied by the geoneutrino observations of KamLAND (KL) and Borexino (BX) with the ranges of radiogenic heating predicted by the cosmochemical (CC) and geophysical (GP) models and with the surface heat flow. Minimum implied heating results from a homogeneous distribution of heat-producing elements in the mantle. Maximum implied heating results from an enriched layer of heat-producing elements at the core-mantle boundary overlain by a homogeneous mantle with depleted MORB-source mantle composition.

If the two observatories sample different mantle signals, it is tempting to speculate that the higher Borexino value is due in part to proximity to the large low shear velocity province beneath the African continent (Garnero and McNamara, 2008) with enriched concentrations of heat-producing elements.

The successful measurements of geoneutrinos by KamLAND and Borexino prompt an evaluation of radiogenic heating measurements from future observatories. Of near term interest is the SNO+ project, which is deploying a detector in a mine (46.47_N, 278.80_E) near Sudbury, Canada at a depth of ≈6 km.w.e. (Chen 2006). It plans to monitor ≈6 _ 1031 free protons with >9000 photomultiplier tubes, collecting scintillation light from 54% of solid angle. Figure (7) shows the energy spectrum of antineutrino interactions predicted at the Sudbury site, assuming a geoneutrino rate of 49 TNU with a signal averaged Th/U ratio of 4.1 and a reactor background rate of 40 TNU in the geoneutrino energy region. After an exposure of 3 TNU_1, these rates, assuming 10 TNU from the mantle, 15% uncertainty in the geoneutrino rate from the crust, and ignoring the negligible nonneutrino background, project a 12% measurement of the geoneutrino rate and ≈80% measurement of the mantle geoneutrino rate (Dye, 2010). The latter corresponds to estimates of global and mantle radiogenic heating equal to 20 _ 10 TW and 12 _ 10 TW, respectively. Increasing exposure gains little, as the _10 TW uncertainty is not much larger than the _8 TW systematic limit for the given assumptions. Another project, LENA, plans to deploy a much larger detector, either in a mine (63.66_N, 26.05_E) near Pyhäsalmi, Finland or under the French-Italian Alps (45.14_N, 6.69_E) near Modane, France (Wurm *et al*., 2012). The high statistics possible with this project allows measurement of the signal averaged thorium-to-uranium mass ratio to 20% or better (Wurm *et al*., 2012). Unfortunately, model predictions of the signal averaged thorium-touranium ratio at the existing and the future continental locations have relatively small differences (<3%). Moreover, the rate shift and spectral distortion introduced by assuming the average neutrino survival probability (Fig. 5) overestimates mantle signal and underestimates the Th/U ratio. These effects are enhanced at locations with proximity to increased levels of uranium and thorium, such as the Sudbury basin (Perry *et al*., 2009).

Deploying a detector in the ocean basin far from continental crust allows maximal sensitivity to the geoneutrino signal from the mantle (Rothschild *et al*., 1998; Enomoto *et al*., 2007; Dye 2010; Gando *et al*., 2011; Mareschal *et al*., 2011). The predicted signal from the crust over much of the Pacific is less than 4 TNU (Enomoto *et al*., 2007). This low crust rate reduces the systematic uncertainty of the mantle signal to ≈1 TNU, which is comparable to that introduced by the _10% precision of the chondritic abundances of uranium and thorium. Figure (8) plots the expected total geoneutrino signals with systematic uncertainty only, assuming a homogeneous mantle, for an oceanic, existing, and continental site as a function of radiogenic heating. Assuming radiogenic heating measurements of 20 TW, the overlap of the cosmochemical and geophysical model ranges, estimates the ultimate precisions from a single observation. The oceanic, existing, and continental observations expect to measure 20 TW of radiogenic heating with uncertainty no better than ≈15%, ≈30%, and ≈40%, respectively. Clearly, the oceanic observation offers the best resolution of radiogenic heating and the tightest constraints on geological models. Moreover, the oceanic observation potentially offers discrimination by geoneutrino signal thorium-to-uranium ratio. The cosmochemical and geophysical models predict signal averaged thorium-to-uranium ratio ranges at the oceanic observatory of 3.2–3.6, and 3.5–3.7, respectively.

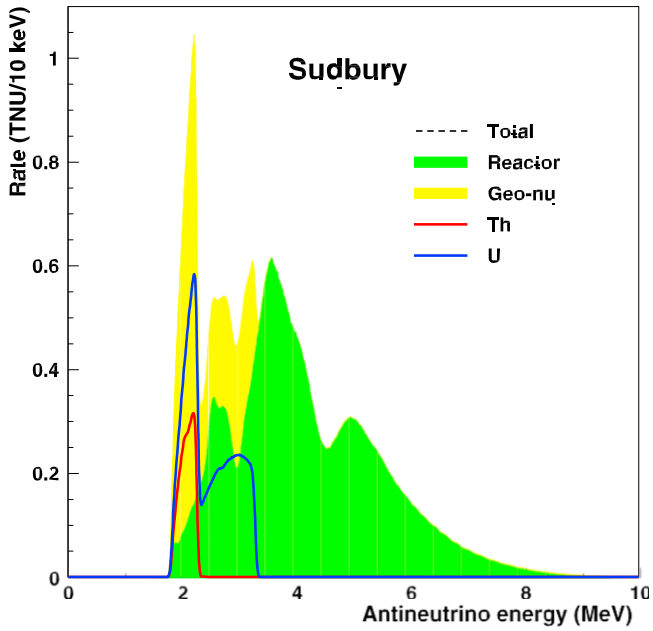

Figure (7). The predicted antineutrino energy spectra for Sudbury, Canada, showing the contributions from geoneutrinos (U and Th) and nuclear reactors. The spectra assume a detected energy resolution of dEne = 7% Ene _1/2.

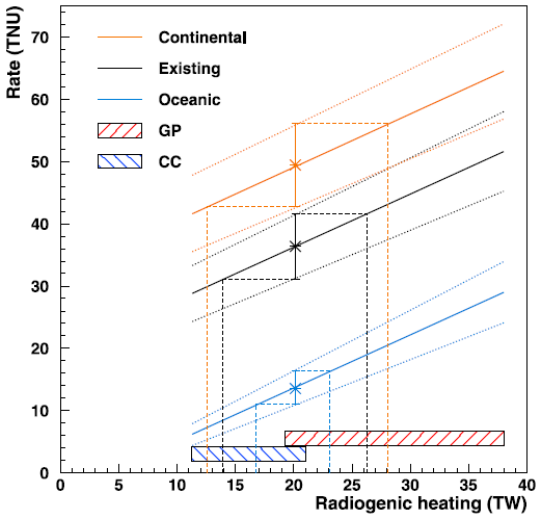

Figure (8). Expected geoneutrino signals (solid lines) with systematic errors (dotted lines) expected at an oceanic (blue), existing (black), and continental site (brown) as a function of radiogenic heating. Assuming a terrestrial radiogenic heating of 20 TW, the systematic uncertainty introduces error (dashed lines) of 15% at the oceanic site, 30% at an existing site, and 40% at a continental site.

Distinguishing these different values requires analysis of the shape of the interaction energy spectrum, which appears possible with sufficient exposure (Wurm *et al.*, 2012). Discriminating the geoneutrino signal rates predicted by the geological models at the oceanic site becomes a statistical issue of detector exposure. Constraining the model end-members requires a relatively modest exposure of about 2 TNU_1. Error in the mantle geoneutrino measurement remains dominated by statistics for exposures of 20–50 TNU_1, depending

inversely on the level of radiogenic heating. A project to build and operate a movable deep ocean antineutrino observatory capable of such exposures is under discussion (Dye *et al*., 2006; Learned *et al*., 2008).

Conclusion

This review presents the science and status of geoneutrino observations, including the prospects for measuring the radioactive power of the planet. Present geoneutrino detection techniques provide sensitivity to the main heatproducing nuclides ^{238}U and ^{232}Th. Techniques presenting directional capability and sensitivity to lower-energy geoneutrinos from ^{235}U and ^{40}K require development. Existing observations with limited sensitivity to geoneutrinos from the mantle constrain radiogenic heating to 15–41 TW, assuming a thorium-to-uranium ratio and a homogeneous mantle. This range of acceptable values is comparable to those estimated by geological models (11–38 TW) and planetary cooling (13–37 TW). Future observations with greater sensitivity to geoneutrinos from the mantle offer more precise radiogenic heating assessments, approaching 15% at oceanic locations. More accurate evaluations of the geoneutrino energy spectrum access the unmeasured thorium- to-uranium ratio, helping to discriminate Earth models if signals have dominant mantle contributions. At continental locations, including the sites for several future observatories, the predicted mantle geoneutrino contribution is ≈20% of the total. Observations at oceanic locations far from continents provide measurements of mantle geoneutrinos that lift the veil of uncertainty obscuring the radioactive power of the planet.

Acknowledgments

We express our gratitude for useful discussions Dr C. Bonadiman, L. Carmignani, M. Coltorti, S. Enomoto, K. Inoue, E. Lisi, T. Mitsui, B. Ricci, N. Sleep, A. Suzuki, and F. Villante. The manuscript benefited from constructive reviews and comments by A.N. Onymous and M.Ozima. This work was partially supported by ISAPP (International Sciences for Astroparticle Physic).

References

Albarede, F., (2003). *Geochemistry: an introduction*, Cambridge University Press 248 pp.

Alimonti G. *et al*., (2002). BOREXINO Collaboration, Science and technology of Borexino: a real-time detector for low energy solar neutrinos, *Astroparticle Phys*. 16 205-234. (23) R.D. Van der Hilst, H. Kárason, Compositional heterogeneity in the bottom 1000 km of Earth's mantle: towards a hybrid convection model, Science 283 (1999) 1885-1888. (24) L.H. Kellogg, B.H. Hager, R.D. Van der Hilst, Compositional stratification in the deep mantle, Science 283 (1999) 1881-1884.

Chen, M. C., (2006), *Geo-neutrinos in SNO+*, Earth Moon Planets, 99, 221–228.

Cowan, C. L., Reines, Jr. F., Harrison, F. B., Kruse, H. W. and McGuire, A. D., (1956). Detection of the Free Neutrino: A Confirmation, *Science* 124 103-104.

Dye, S. T., *et al*. (2006), Earth radioactivity measurements with a deep ocean antineutrino observatory, *Earth Moon Planets*, 99, 241–252.

Dye, S. T. (2010), Geo-neutrinos and silicate earth enrichment of U and Th, Earth Planet. *Sci. Lett*., 297, 1–9.

Dziewonski, A. M. and Anderson, D. L., (1981). Preliminary reference Earth model, *Physics Earth Planet*. Int. 25 297-356.

Eguchi K. *et al*., (2003). KamLAND Collaboration, First Results from KamLAND: Evidence for Reactor Antineutrino Disappearance, *Phys. Rev. Lett*. 90 0218021-0218026 (arXiv:hep-ex/0212021).

Enomoto, S., *et al*., (2007). Neutrino geophysics with KamLAND and future prospects, Earth Planet. *Sci. Lett*., 258, 147–159.

Gando, A., *et al*., (2011). Partial radiogenic heat model for Earth revealed by geoneutrino measurements, *Nat. Geosci.*, 4, 647–651, doi:10.1038/NGEO1205.

Ganero, E. J., and A. K. McNamara, (2008). Structure and dynamics of Earth's lower mantle, *Science*, 302, 626-628.

Jochum, K. P., Hofmann, A. W., Ito, E., Seufert, H. M., White, W. M., K., (1983). U and Th in mid-ocean ridge basalt glasses and heat production, K/U and K/Rb in the mantle, *Nature* 306 431-436.

Learned, J. G., S. T. Dye, and S. Pakvasa, (2008). Hanohano: A deep ocean anti-neutrino detector for unique neutrino physics and geophysics studies, *in Proceedings of the XII International Workshop on Neutrino Telescopes*, Venice, March 6–9, 2007.

Mantovani, F., Carmignani, L., Fiorentini, G. and Lissia, M., (2004). Antineutrinos from Earth: A reference model and its uncertainties, *Phys. Rev*. D 69 0130011-01300112 (arXiv:hep-ph/0309013).

Mareschal, J.-C., *et al*., (2011), Geoneutrinos and the energy budget of the Earth, *J. Geodyn*., 54, 43–54.

Pontecorvo, B., (1946). Inverse Beta Process, National Research Council of Canada, Division of Atomic Energy. Chalk River, *Report PD-205*, reprinted in: J. N. Bahcall, R. Davis, Jr., P. Parker, A. Smirnov, and R. Ulrich (Eds.), Solar Neutrinos, The First Thirty Years, Westview Press, 2002.

Raghavan, R. S., Schoenert, S., Enomoto, S., Shirai, J., Suekane, F. and Suzuki, A., (1998). Measuring the Global Radioactivity in the Earth by Multidetector Antineutrino Spectroscopy, *Phys. Rev. Lett*. 80 635-638.

Rothschild, C. G., M. C. Chen, and F. P. Calaprice, (1998). Antineutrino geophysics with liquid scintillator detectors, *Geophys. Res. Lett*., 25, 1083–1086.

Togashi, S., Imai, N., Okuyama-Kusunose, Y., Tanaka, T., Okai, T., Koma, T., Murata, Y., (2000). Young upper crustal chemical composition of the orogenic Japan Arc, *Geochem. Geophys. Geosyst*. 1 (11) 10.129/2000GC00083.

Wurm, M., *et al*., (2012). The next-generation liquid-scintillator neutrino observatory LENA, *Astropart. Phys*., 35, 685–732.

Zartman, R. E., Haines, S., (1988). The Plumbotectonic Model for Pb Isotopic Systematics among Major Terrestrial Reservoirs - a Case for Bi-Directional Transport, *Geochim. Cosmochim. Acta* 52 1327-1339.

Zhao, D., Horiuchi, S., Hasegawa, A., (1992). Seismic velocity structure of the crust beneath the Japan Islands, *Tectonophysics* 212 289-301.